Generation of a High-Velocity Jet in the Electrothermal Explosion of Conductive Ceramic Powders

H. Tamura, M. Konoue, Y. Ikeda, T. Soda, and A.B. Sawaoka

The electrothermal explosion spraying of conductive ceramic powders was characterized according to the electric and gas dynamic behavior of heated powders. Optical observation revealed the generation of the jetting with a leading velocity over 3 km/s. The velocity depended on the shape of the jet and the energy supplied to the powder. The heating process was related to the jetting process of the heated powders. The total electric energy supplied to the powder was two to three times the theoretical amount needed to melt the powder. Such electric energy was used for heating and accelerating the powder. This spray technique is characterized with the high-velocity jet consisting of high-pressure gas and molten ceramic particles.

1. Introduction

Coatings composed of refractory ceramics with melting points higher than 3000 K have been sprayed from carbides and borides by the electrothermal explosion method (Ref 1, 2). These coatings are dense with the deposition of molten particles and mixing of coating and substrate materials (Ref 2). However, the spraying process has not been characterized sufficiently to understand the technique. The coating adhesion to the substrate depends on many factors including the coating density, chemical composition, and microstructure (Ref 3) that have resulted from the heating of spray particles, the surrounding atmosphere, and the impact velocity. In this technique, the electrical heating of powders had been estimated by electrical measurements (Ref 2), and other spraying conditions of the particles had not been established. This spray process is characterized by time-resolved optical observation of the explosion.

2. Experimental Setup

The ceramic powder was charged under argon gas in a container which was concentrically composed of an inner polyethylene tube and an outer cylindrical metal jacket. The schematic cross section of the container is shown in Fig. 1. The jacket had a window 4 mm wide by 40 mm long. The powders used were zirconium boride, ZrB_2 (bulk density, 6.1×10^3 kg/m^3; particle size, <10 μm; purity, 99.5%), and tantalum carbide, TaC (bulk

H. Tamura, M. Konoue, Y. Ikeda, and **T. Soda,** Department of Materials Science and Engineering, Tokyo Institute of Technology, Nagatsuta 4259, Midori-ku, Yokohama 226, Japan; **A.B. Sawaoka,** Materials and Structures Laboratory, Tokyo Institute of Technology, Nagatsuta 4259, Midori-ku, Yokohama 226, Japan.

density, 14.4×10^3 kg/m^3; particle size, 2 to 4 μm, purity, 99.5%). A pair of tungsten electrodes was fitted into both ends of the container. The container was placed in a vacuum chamber and connected to the electrical contacts of the electrical circuit (Ref 1). High pressure gas and molten particles generated by electrical heating of the powder should be ejected from the tube through the window during the electrothermal explosion. A jet composed of such gas and particles was photographed with the schlieren technique. The light beam used in this technique radiated the space adjacent to the window. A viewing area was obtained (Fig. 1).

The light beam of 488 nm in wavelength coming from an argon laser was enlarged in diameter with an object lens (focal
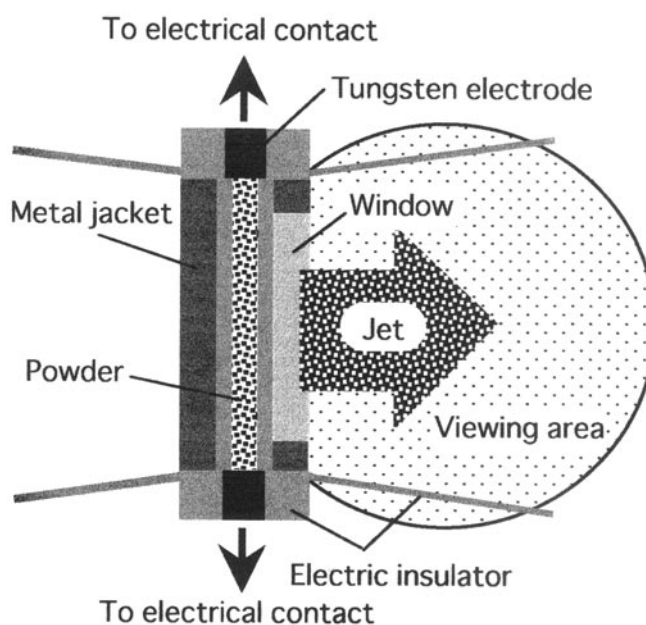
Fig. 1 Schematic of a sectioned powder container and viewing area of schlieren photography

length, 4.7 mm) and a plano-convex lens. The light beam was introduced into the vacuum chamber via a polymethyl methacrylate (PMMA) window, as shown in the schlieren system in Fig. 2. After passing by the container in the chamber, the beam exited the chamber through another window and was focused with another plano-convex lens to pass through an iris diaphragm of 1 mm in diameter. A neutral density filter and a bandpass filter (central wavelength, 488 nm; band width, full-width at half maximum, 3 nm) were placed between the iris and lens. The laser beam was finally imaged by a high speed camera (Model UL-TRANAC FS-501, Imco Electro Optics Ltd., UK). A master trigger was used to sequentially start the digital oscilloscope, electrical heating of a powder, and the high speed camera.

The voltage applied between the pair of tungsten electrodes was estimated from the measurements using a high-voltage probe (Model HV-P30, Iwatsu Co., Japan) connected to the electrical contacts of the chamber and a Rogowski coil (made and calibrated by the authors) detecting a current flow in the powder (Ref 1). Based on the voltage and current obtained, the apparent resistance of the powder and the electric power supplied to the powder were calculated. The electrical heating of the powder was evaluated from comparison of the energy consumed in the powder to that theoretically needed to only melt the powder.

3. Experimental Results and Discussion

3.1 *Jetting of Tantalum Carbide*

Fifty millimeters of tantalum carbide (TaC) powder of 46.0% relative density was charged into a high-density polyethylene tube of 0.94×10^3 kg/m^3 density, with outer and inner diameters of 6 and 3 mm, respectively. The schlieren photographs taken are shown in Fig. 3. Each exposure time and interframe period was 0.8 and 3 µs, respectively. They are arranged alphabetically
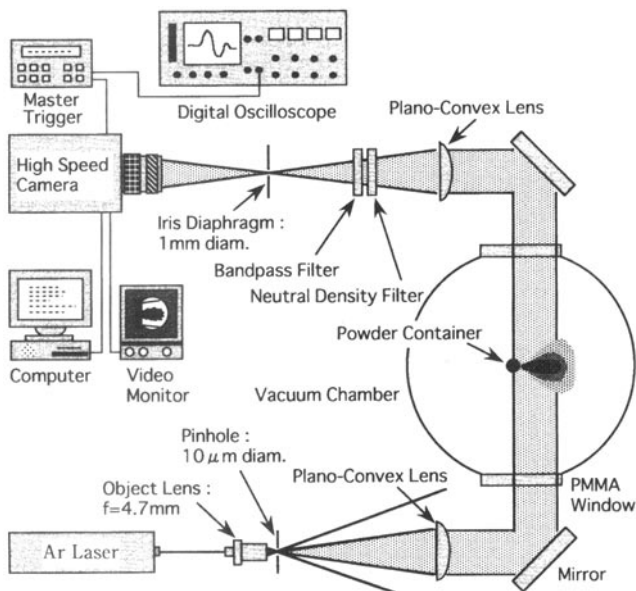
Fig. 2 Schematic of schlieren photography observing jetting under electrothermal explosion of powders

in a time sequence. The first frame (a) was taken 31 µs after the start of current discharge which was 60 µs on the time scale shown in Fig. 4(a). In the second frame (b), a small dark spot can be observed as indicated with the arrow. It is enlarged in the third frame (c) after 3 µs. Thus, the dark region extended sequentially
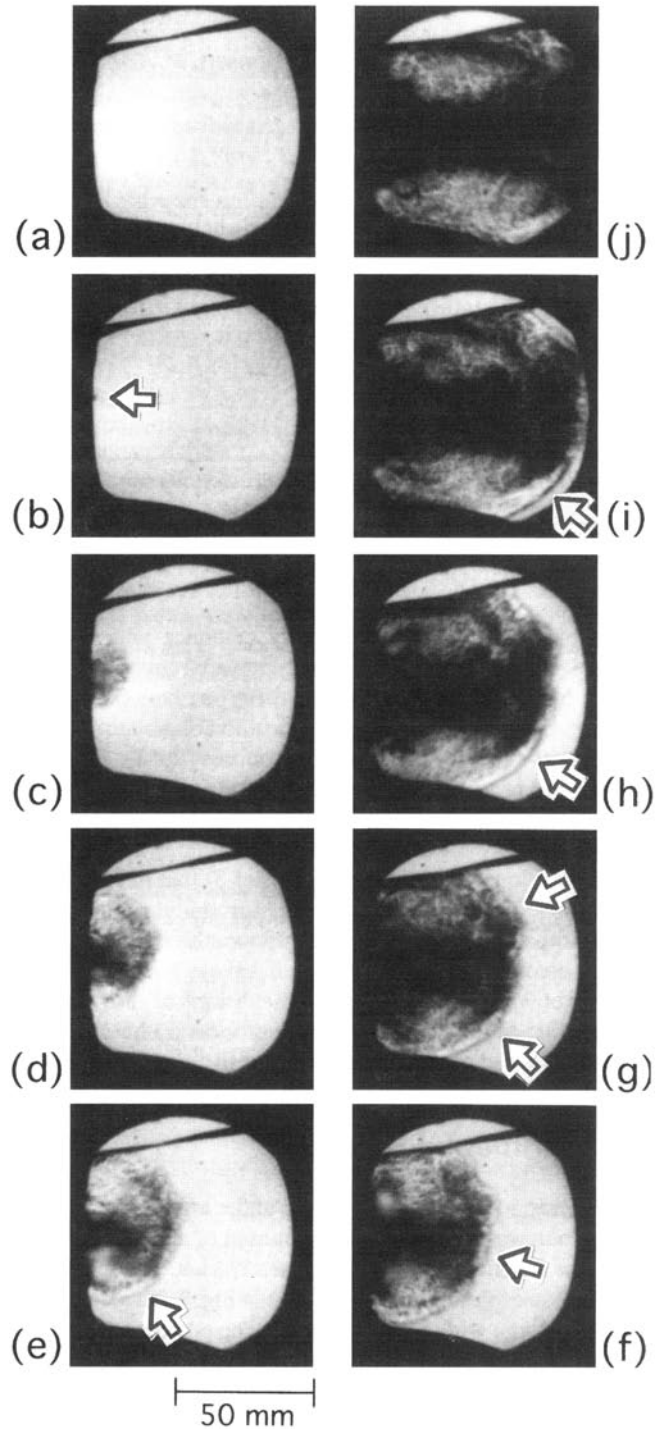
Fig. 3 Schlieren photographs showing the explosion of tantalum carbide powder. They are arranged alphabetically in a time sequence. Each exposure time and interframe period were 0.8 and 3 µs, respectively. The arrows indicate the appearance of explosions in frame (a) and shock wave fronts in frames (e) to (i).

from the window in an outward direction. In addition, thin dark lines were detected around the dark region, as indicated with the arrows in frame (e) to (i). The moving speed of the lines perpendicular to the axis of the powder container was estimated at >3 km/s due to the time-of-flight. In addition, these lines were accompanied by a narrow bright region behind them, which is interpreted as shock waves by comparison to other schlieren photographs. Thus, these features are interpreted as shock-wave fronts which propagated in the air.

Corresponding to these photos, the voltage and discharge current applied to the powder were also measured and are shown in Fig. 4(a). The apparent resistance and electric power calculated are shown in Fig. 4(b) and (c), respectively. The resistance and power obtained at the time when a frame was taken is marked with the frame code. The initial voltage applied was 8.3 kV and lasted for 55 μs; then it was followed by the current dis-

charge which happened at 60 μs on the time scale. The resistance exponentially decreased, while the current discharged. This event was caused by the heating of argon gas, removing of oxidized surface layers of powder particles, and enlarging the con-
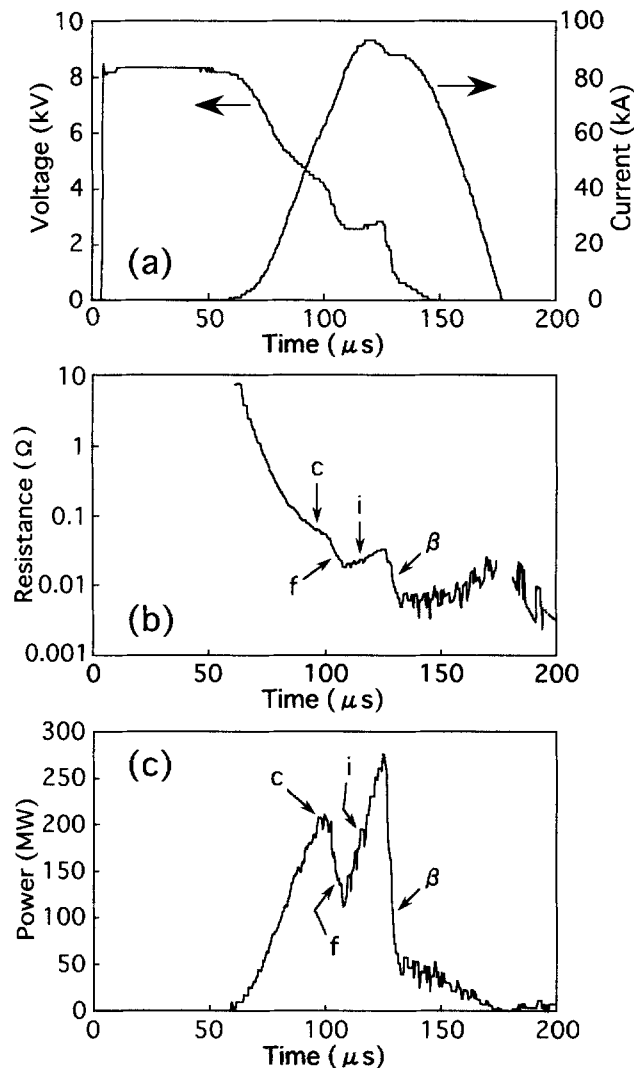
Fig. 4 Electrical characteristics of the explosion shown in Fig. 3. The applied voltage and current is shown as a function of time in (a). The apparent resistance of the powder and the electric power supplied are also shown in (b) and (c), respectively. The resistance and power obtained when the frames in Fig. 3 were photographed are marked with the corresponding frame order.
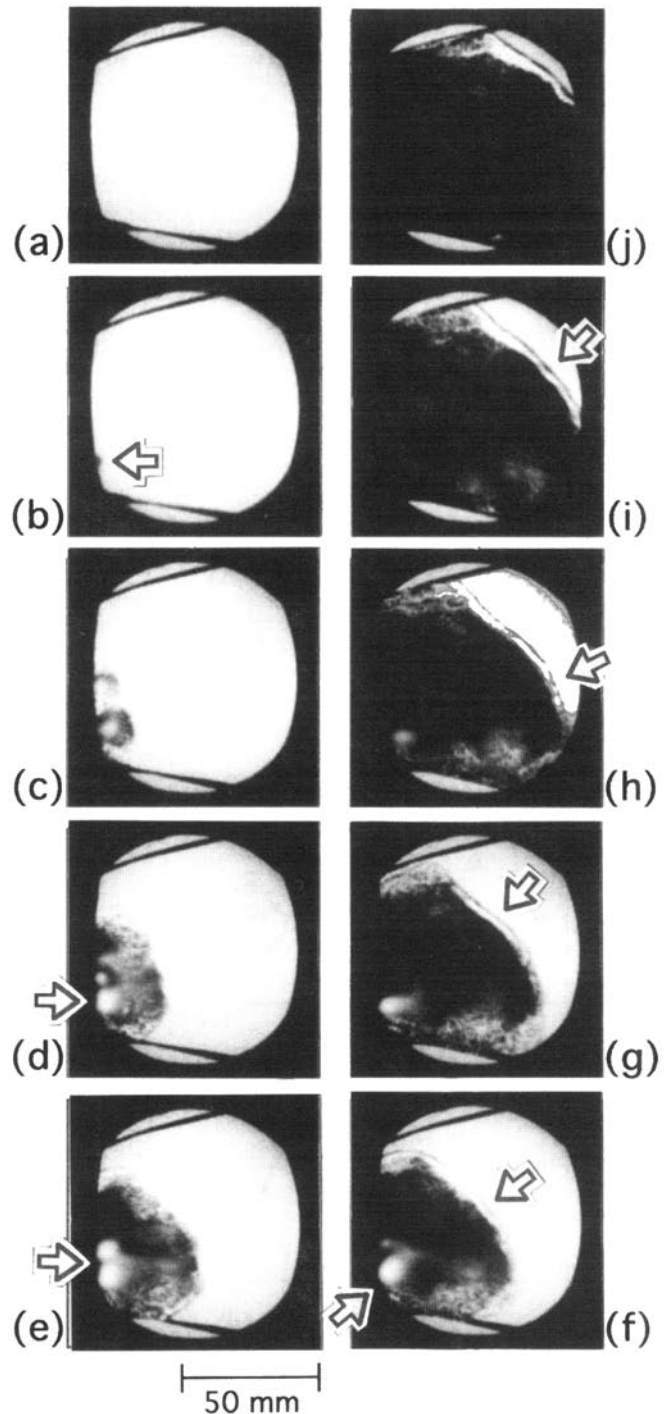
Fig. 5 Schlieren photographs showing the explosion of zirconium boride powder. They are arranged alphabetically in a time sequence. Each exposure time and interframe period was 0.7 and 3 μs, respectively. The arrows indicate the appearance of explosions in frame (b), bright radiation in frames (d) to (f), and shock wave fronts in frames (f) to (i).

tact surfaces of the particles. These phenomena contributed to a decrease in the apparent resistance.

On the other hand, since TaC has metallic resistivity (Ref 4), the resistances of particles must be increased with a temperature increase caused by Joule heating. Thus, such a resistance increase of the particles should begin to contribute to the total apparent resistance of the powder, as the current discharges. The decreasing rate of the apparent resistance approximately 80 to 100 μs is smaller than that obtained earlier than 80 μs. This arises due to Joule heating of the particles. In fact, the electric power supplied to the powder increased in this period, (Fig. 4c). From 100 μs, however, the resistance started to decrease rapidly again, and then the power also decreased. This rapid decrease is due to the removal of some heated particles with high resistivity from the container hence leaving heated gas within the container with low resistivity. Since frames (e) and (f) were taken during

this event, the central, dark region would contain a cluster of such heated particles. Although the cluster of such particles still extended outward, as shown in frames (h), (i), and (j), the resistance and power increased again. It is assumed that the other particles remaining in the container were heated further and obtained higher resistivity.

At 130 μs, the resistance and power decreased rapidly again, as marked with β in Fig. 4 (b) and (c). This event occurred outside the view of the photo frames. However, it is considered that (a) many particles can be heated and ejected outside the container so that gas with low resistivity would be left inside and/or (b) another gas ejecting behind the shock wave might induce a new current path between the electrical contacts outside the container. The electric energy put into the powder until 130 μs is estimated to be 9.4 kJ while the theoretical energy necessary to melt just the powder is 4.6 kJ (Ref 2).

3.2 Jetting of Zirconium Boride

Fifty millimeters of ZrB_2 powder of 56.7% relative density was charged into a low-density polyethylene tube of 0.91×10^3 kg/m^3 density, with outer and inner diameters of 5 and 3 mm, respectively. The schlieren photographs taken are shown in Fig. 5. Each exposure time and interframe period were 0.7 μs and 3 μs, respectively. They are arranged alphabetically in a time sequence. The second frame (b) was taken 31 μs after the start of current discharge which was 50 μs on the time scale shown in Fig. 6(a). The frames (b) and (c) taken at 81 μs and 84 μs show the appearance of a small dark spot and its extension, respectively. The resistance obtained from approximately 65 μs to 85 μs seems to be affected by the increase of resistivity of heated ZrB_2 particles in the container (as mentioned for the case of TaC). From 85 to 93 μs, the resistance decreased more rapidly and was accompanied by a power decrease. Thus, the powder particles that heated enough to have high resistivity were ejected in the extending dark region as shown in frames (d), (e), and (f). In these frames, a bright region, surrounded by a dark region, is detected at the bottom side of the window and is marked with an arrow. This bright region was likely due to radiation from current discharge in the gas or heated particles.

In addition, a thin dark line (also marked) was found adjacent to the periphery of the extending dark region. The narrow bright-region is between the line and inner dark region. As time passed from frames (h), (i), and (j), the line became more defined. According to its moving speed of more than 3 km/s, it can be classified as a shock wave front. During this period, resistance was nearly constant, and power increased. Thus, energy was still supplied to the powder particles left inside the container. At 119 μs, however, the resistance and power decreased rapidly again, as marked with β in Fig. 6(b) and (c). The electric energy input to the powder until that time was estimated at 10.8 kJ; the theoretical one for melting just the powder is 4.2 kJ (Ref 2). The input energy was 2.6 times the theoretical amount required to melt the powder.

In this series of experiments, the explosion caused a shock velocity in excess of 5 km/s, Fig. 7. The preparation of the powder was the same as above, but the relative density was only 59.1%. Frame (a) shows the explosion happened at the center of the window, and frames (d), (e), and (f) show the outward extension of the central dark region and shock waves marked with arrows. Such ejection is characterized by the central dark-colored
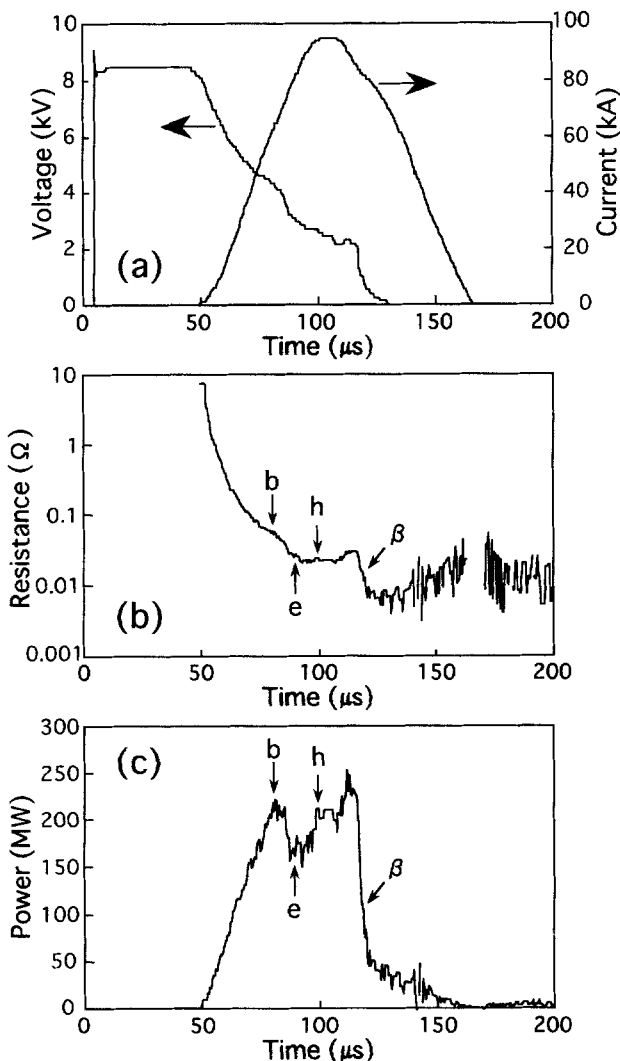
Fig. 6 Electrical characteristics of the explosion shown in Fig. 5. The applied voltage and current is shown as a function of time in (a). The apparent resistance of the powder and the electric power supplied are also shown in (b) and (c), respectively. The resistance and power obtained when the frames in Fig. 5 were taken are marked with the corresponding frame order.

protrusion, but its front is not as clearly distinguished as the other shock fronts shown in Fig. 3 and 5. Such an indistinctive feature is due to a 3.5 mm travel, for example, the displacement of the shock front even during the exposure time of 0.7 μs.

Figure 8 illustrates the electric features of this explosion. If the power is integrated until the central protrusion is distinguished, as shown in Fig. 7 (d), the electric energy is calculated as 6.6 kJ. The explosion extended until that time and corresponded to the one shown in Fig. 5(f). The energy supplied until the time corresponding to Fig. 5(f) is 5.7 kJ. The generation of such high-velocity jetting is therefore caused by the localization of the jetting protrusion and the higher energy supply. Further increase of jetting velocity is expected due to the optimization of the shapes of the container, window, and the energy input to the powder. The total electrical energy consumed until 125 μs was

12.2 kJ, this being 2.8 times the theoretical energy of 4.4 kJ for melting only the powder.

3.3 Estimation of Jetting Velocities

The shock wave velocity perpendicular to the axis of the container is summarized in Fig. 9. The velocities obtained above and those found in the other three explosions are shown as a function of distance from the window. The container, a high-density polyethylene tube, with outer and inner diameters of 8 and 3 mm, respectively, was also used to generate a TaC jet. The shock velocity was approximately 3.5 km/s and is comparable to that obtained for tubes 6 mm in outer diameter. Although the shock wave and associated gas flow changed spatially in time, they can be evaluated by a one
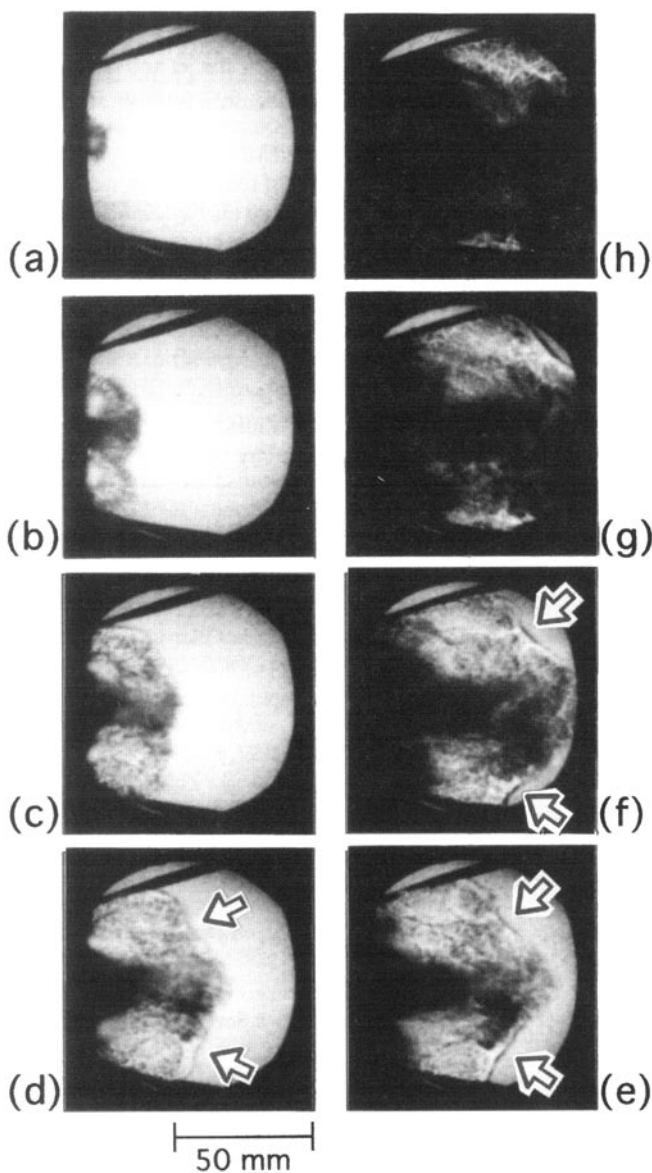
Fig. 7 Schlieren photographs showing the explosion of zirconium boride powder. They are arranged alphabetically in a time sequence. Each exposure time and interframe period were 0.7 and 3 μs, respectively. The arrows indicate the shock wave fronts in frames (d) to (f).
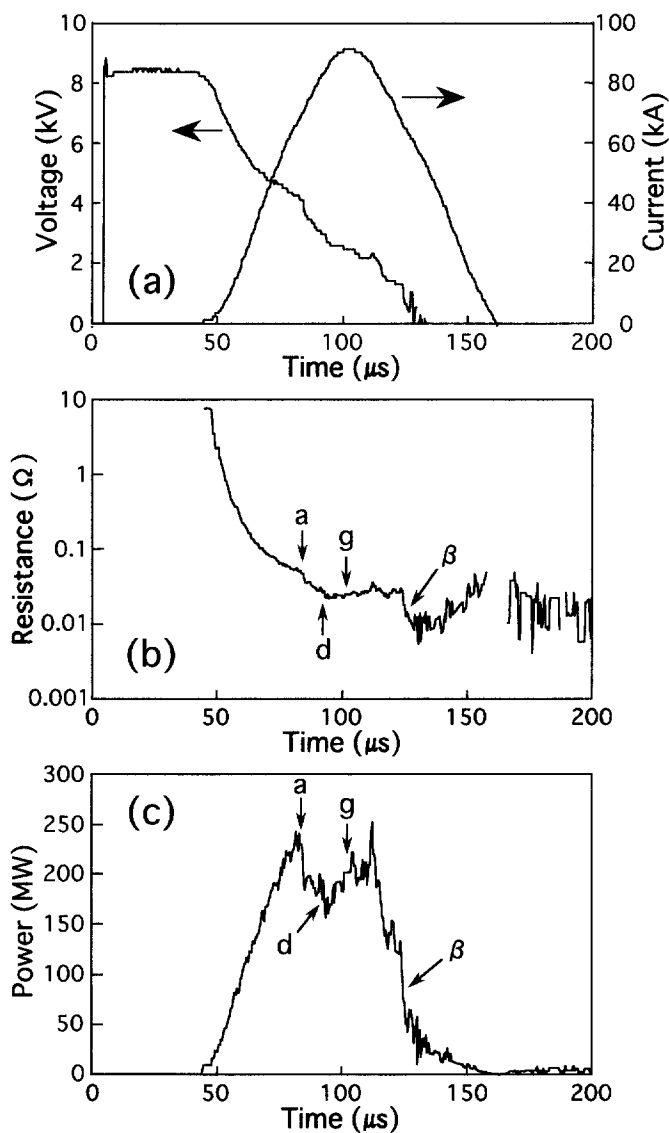
Fig. 8 Electrical characteristics of the explosion shown in Fig. 7. The applied voltage and current is shown as a function of time in (a). The apparent resistance of the powder and the electric power supplied are also shown in (b) and (c), respectively. The resistance and power obtained when the frames in Fig. 7 were taken are marked with the corresponding frame order.

△ TaC (O.D. 6mm)   ● TaC (O.D. 8mm)
○ TaC (O.D. 6mm)   ◆ ZrB2 (O.D. 5mm)
□ TaC (O.D. 6mm)   ■ ZrB2 (O.D. 5mm)
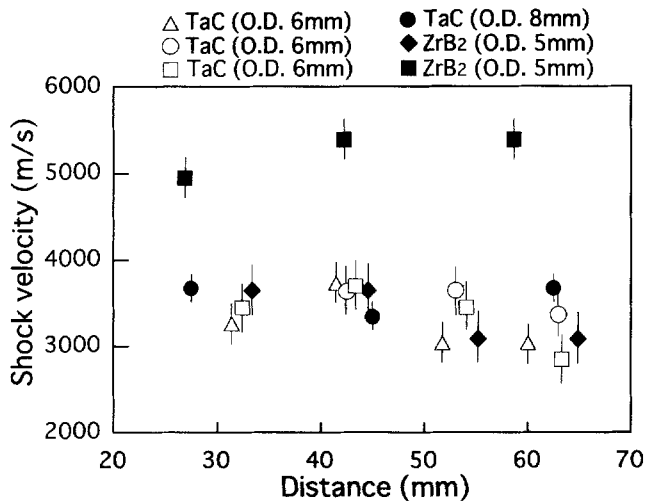
Fig. 9 Shock wave velocities as a function of distance from the container window. The shock velocity in excess of 5 km/s for the case of ZrB2 marked by ■ is caused by the localization of the jetting protrusion and the higher energy supply to the powder.

dimensional approximation that describes them in the region close to the shock front for an instant. In terms of approximation, it is thought that the shock wave is followed by high speed air flow compressed by another ejecting gas flow working as a piston.

Based on a one-dimensional shock velocity obtained for one interframe of 3 μs, the velocity of the piston, U_p, is calculated with Rankine-Hugoniot relations of gas prepared for strong shock wave; this is described as follows (Ref 5):

$$U_s = A_1 \sqrt{\frac{(\gamma + 1) P_2}{2\gamma P_1}}$$

(Eq 1)

$$U_p = A_1 \sqrt{\frac{2 P_2}{\gamma (\gamma + 1) P_1}}$$

(Eq 2)

where U_s, A, P, and γ are shock velocity, sound velocity, pressure, and specific heat ratio, respectively. The subscripts, 1 and 2, denote the initial steady state in front of the shock and the compressed steady state behind the shock, respectively. Equations 1 and 2 give the relation of U_p and U_s:

$$U_p = \frac{2 U_s}{\gamma + 1}$$

(Eq 3)

Using the representative U_s of 3.6 km/s at 43 mm for TaC shown in Fig. 9 and $\gamma = 1.403$ for air, for example, the piston ve-

locity, U_p, which is the velocity of the jet driving the compression of air, is estimated at 3.0 km/s. The pressure ratio as P_2/P_1 is also calculated as ~130 for $A_1 = 343$ m/s at 20 °C in Eq 1. The highest shock velocity of 5.4 km/s which occurred for the case of ZrB2 jetting corresponds to 4.5 km/s in the jetting velocity. Consequently, it is found that the jetting shape influences its velocity.

4. Conclusions

The electrothermal explosion spraying of conductive-ceramic powders was investigated with time-resolved measurements which characterized the electric and gas dynamic behavior of powders under a large current discharge. The heating process of the powders was closely related to the jetting of exploded powders. The supply of the electric energy to the powder caused jetting with a leading velocity of more than 3 km/s.

The velocity depends on the shape of the jet and the electric energy supplied to the powders. Thus, optimization of the jet shape increases velocity. Using the present container, the total electric energy was 2 to 3 times the theoretical energy needed to melt the powder only. Modification of the container would also change the total amount of the supplied energy. Therefore, this spray process is based on high velocity jetting consisting of high pressure gas and molten ceramic particles.

References

1. H. Tamura, M. Nagahama, Y. Tanabe, and A.B. Sawaoka, Spraying of Zirconium-Diboride Powder by an Electrical Column Explosion Technique and Its Mechanism, *J. Appl. Phys.*, Vol 75, 1994, p 4695-4703

2. H. Tamura, M. Konoue, and A.B. Sawaoka, Zirconium Boride and Tantalum Carbide Coatings Sprayed by Electrothermal Explosion of Powders, *J. Therm. Spray Technol.*, Vol 6, 1997, p 463-468

3. C.K. Lin and C.C. Berndt, Measurement and Analysis of Adhesion Strength for Thermally Sprayed Coatings, *J. Therm. Spray Technol.*, Vol 3, 1994, p 75-104

4. R.B. Kontel'nikov, S.N. Basl'ikov, Z.G. Galiakbarov, and A.I. Kastanov, *High Refractory Elements and Compounds*, R.B. Kontel'nikov, S.N. Basl'ikov, Z.G. Galiakbarov, and A.I. Kastanov, Ed., Nisso-tsuushinnsha, Wakayama, 1977, p 56-57 (in Japanese)

5. H.W. Liepmann and A. Roshko, *Elements of Gasdynamics*, T. Karman and C.B. Millican, Ed., John Wiley & Sons, Inc., 1960, p 65